Mechanism of Nucleic Acid Phosphodiester Bond Cleavage by Human Endonuclease V: MD and QM/MM Calculations Reveal a Versatile Metal Dependence

Rajwinder Kaur[a] and Stacey D. Wetmore[a]*

[a]*Department of Chemistry and Biochemistry, University of Lethbridge, 4401 University Drive West, Lethbridge, Alberta, Canada T1K 3M4*

*E-mail: stacey.wetmore@uleth.ca. Tel.: (403) 329-2323.

Keywords: EndoV, phosphodiester bond, metal, RNA, QM/MM, MD, nuclease, mechanism

Abstract: Human endonuclease V (EndoV) catalytically removes deaminated nucleobases by cleaving the phosphodiester bond as part of RNA metabolism. Despite being implicated in several diseases (cancers, cardiovascular diseases, and neurological disorders) and potentially being a useful tool in biotechnology, details of the human EndoV catalytic pathway remain unclear due to limited experimental information beyond a crystal structure of the apo-enzyme and select mutational data. Since a mechanistic understanding is critical for further deciphering the central roles and expanding applications of human EndoV in medicine and biotechnology, molecular dynamics (MD) simulations and quantum mechanics-molecular mechanics (QM/MM) calculations were used to unveil the atomistic details of the catalytic pathway. Due to controversies surrounding the number of metals required for nuclease activity, enzyme–substrate models with different numbers of active site metals and various metal–substrate binding configurations were built based on structural data for other nucleases. Subsequent MD simulations revealed the structure and stability of the human EndoV–substrate complex for a range of active site metal binding architectures. Four unique pathways were then characterized using QM/MM that vary in metal number (one versus two) and modes of substrate coordination (direct versus indirect (water-mediated)), with several mechanisms being fully consistent with experimental structural, kinetic, and mutational data for related nucleases, including members of the EndoV family. Beyond uncovering key roles for several active site amino acids (D240 and K155), our calculations highlight that, while one metal is essential for human EndoV activity, the enzyme can benefit from using two metals due to the presence of two suitable active site binding sites. By directly

comparing one versus two-metal-mediated P–O bond cleavage reactions within the confines of the same active site, our work brings a fresh perspective to the 'number of metals' controversy.

Introduction

Inosine is a key post-transcriptional modification that arises in RNA through various pathways.[1] For example, spontaneous hydrolysis of adenosine (A) or exposure of A to nitrosative stress caused by superoxides and nitric oxide during inflammation can result in inosine.[1-3] Alternatively, imbalanced purine nucleotide metabolism can lead to unexpected inosine triphosphates incorporation into mRNA during transcription, which can result in mutant proteins and inhibit cell viability.[4-5] Although adenosine deaminases also yield inosine as a part of RNA editing to control gene integrity and gene expression,[6-7] hyperedited RNA can occur, resulting in codon changes and thereby altering protein translation.[1] In fact, although balanced adenosine-to-inosine editing is necessary for generating RNA and protein diversity,[8] dysregulated adenosine-to-inosine editing has been connected to 17 different cancers, ranging from colorectal to breast invasive carcinoma,[9-10] as well as other diseases, such as epilepsy,[11] amyotrophic lateral sclerosis (ALS),[12] autism,[13] Alzheimer's,[14] atherosclerosis,[15] and schizophrenia.[16] Therefore, the amount of inosine in RNA must be carefully regulated.

Endonuclease V (EndoV) is a conserved family of enzymes (Figure 1a) that removes deaminated nucleobases, including inosine, by cleaving phosphodiester bonds in nucleic acids.[17-19] Despite highly conserved enzymes generally having similar functions, the bacterial homologue of EndoV is involved in DNA repair,[20] while eukaryotic EndoV is involved in RNA metabolism.[18] EndoV has also been implicated in the development, detection, and treatment of human diseases.[15, 21-27] For example, overexpression of catalytically-inactive EndoV increases sensitivity towards hepatocellular carcinoma treatments.[22] Furthermore, eukaryotic EndoV is overexpressed in carotid atherosclerotic lesions, with enzyme inhibition reducing both plaque size and severity of ischemic strokes.[15] Finally, a genome-wide study of psychiatric disorders demonstrated a significant association between genes that encode EndoV and schizophrenia.[21] To better understand the cellular biochemistry and further enhance disease management, the molecular level details of the mechanism of action used by members of the EndoV family must be uncovered.

Human EndoV catalyzes the Mg^{2+}-dependent cleavage of the second phosphodiester bond on the 3′-side of inosine to generate the 3′-hydroxy and 5′-phosphate products.[28] However, very few details are available about the corresponding mechanism of action. The role and number of metal/s required to cleave the phosphodiester bond are unknown, with no experimental or computational study having investigated the metal dependence of human EndoV activity to date. In fact, the currently available crystal structure of human EndoV (PDB ID: 6OZE, Figure 1b) does not contain the substrate or metal cofactor/s.[28] Furthermore, mutational studies have highlighted the roles of only a few residues, with D52A and Y91A mutations abolishing catalytic activity.[17-18] Comparisons to mouse and bacterial EndoV suggest that Y91 likely occupies the empty space remaining in DNA following base flipping upon substrate binding,[29] while D52 is likely involved in metal binding in the active site.[28] Due to the scarcity of information, there has not yet been a proposal for the human EndoV phosphodiester bond cleavage pathway.

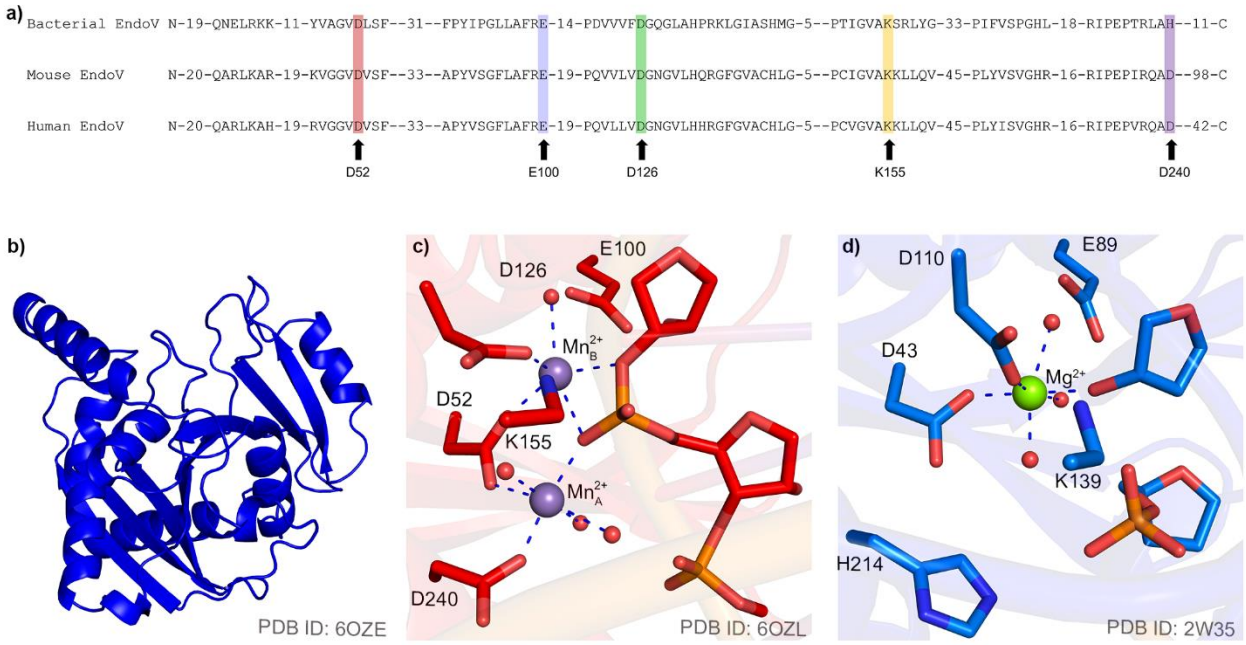

Figure 1. a) Sequence alignment of bacterial, mouse, and human EndoV, with key active site amino acids highlighted. The species and respective GenBank accession numbers used for the alignment are *Thermotoga maritima* and Q9X2H9 for bacterial EndoV, *Mus musculus* and Q8C9A2 for mouse EndoV, and *Homo sapiens* and Q8N8Q3 for human EndoV. The X-ray crystal structure of the b) apo-human EndoV, c) active site for the RC of wild-type mouse EndoV bound to a dsRNA substrate, and d) active site for the PC of wild-type bacterial EndoV bound to a ssDNA substrate.

The prediction of the human EndoV mechanism of action is further complicated by the fact that enzymes from different species have been concluded to use a different number of metals to catalyze the phosphodiester bond cleavage despite high sequence similarity (Figure 1a). For mouse EndoV, X-ray crystallographic data reveal two metals in the active site (Figure 1c).[28] Indeed, the most widely accepted mechanism for nuclease catalysis based on available structural data involves two metals.[28, 30-50] The first metal (M_A^{2+}) activates the water nucleophile for attack at the scissile phosphate, the second metal (M_B^{2+}) promotes leaving group departure through direct or water-mediated coordination, and both metals provide substrate charge stabilization by coordinating to the non-bridging oxygen of the scissile phosphate (Figure 2a).[51] However, the roles and stoichiometry of the metal ions needed for nuclease catalysis has been a controversial issue for almost two decades,[52-66] with proposals for the two-metal mediated mechanism based solely on structural data having been called into question. Indeed, metal concentration dependencies in solution suggest that only one metal may be essential for catalysis by some enzymes despite some endonucleases having two metal-binding sites.[34, 38, 56, 67-68]

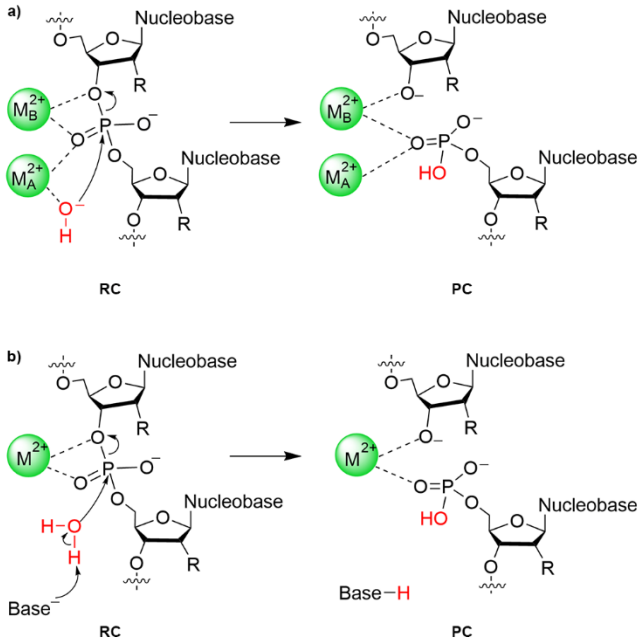

Figure 2. The general proposed mechanism for a) two-metal or b) single-metal mediated phosphodiester bond cleavage by an endonuclease (M^{2+} = metal, and R = H for DNA or OH for RNA).

In contrast to mouse EndoV,[28] bacterial EndoV has been proposed to use a single metal to facilitate P–O bond cleavage,[29, 62] at least in part due to the presence of only one metal in the active site in the X-ray crystal structure of the product complex (PC) of the wild-type enzyme bound to a single-stranded DNA (ssDNA) substrate (Figure 1d). In single-metal dependent nucleases, the function of the first metal in nucleophile activation in the two-metal mediated pathway (M_A^{2+}) has been proposed to be fulfilled by an active site amino acid (Figure 2b),[51, 54-55] such as H214 in bacterial EndoV (Figure 1d).[62] According to sequence alignment, human EndoV contains an Asp residue (D240) in an equivalent position as H214 in bacterial EndoV (Figure 1a). The suggestion that human EndoV may only require one metal is further supported by other single-metal dependent nucleases that have been proposed to efficiently use an Asp residue coupled with one metal to achieve the P–O bond cleavage, such as APE1 (D210, Figure 3a).[57, 63-64] Although an abundance of experimental structural and kinetic studies have proposed that several nucleases use a single metal to cleave the phosphodiester bond,[29, 69-74] computational studies investigating the catalytic mechanisms used by one-metal mediated nucleases are relatively scarce.[57, 62-64]

To address gaps in the EndoV literature, the present work has used a multi-scale computational approach to decipher the general mechanism of action of human EndoV. Initially, since the only available crystal structure does not contain a substrate or metal cofactor/s (Figure 1b),[28] the first model of the human EndoV–substrate complex was constructed. Directed based on existing literature on other nucleases,[28, 32, 69, 74-75] including EndoV from other species,[28-29] molecular dynamics (MD) simulations were then performed in triplicate on complexes with different numbers of active site metals and various metal–substrate binding architectures to gain insights into the structural dynamics of human EndoV. Multiple MD snapshots were chosen that correspond to potentially catalytically-active conformations with differentially aligned active sites as starting points for quantum mechanics-molecular mechanics (QM/MM) calculations within the ONIOM formalism. By characterizing four unique pathways with different numbers of metals (one versus two) and modes of metal–substrate coordination (direct versus indirect), we provide the first atomic-level details of the mechanism of action of human EndoV. Our calculations reveal a rare metal dependence for this enzyme and highlight that nucleases may not all strictly follow traditional one or two-metal dependent mechanisms. As this is only the second computational study of a member of the EndoV family,[62] our work enhances our knowledge of how this broad

family of enzymes process nucleic acids in cells. The fundamental details of the chemistry facilitated by human EndoV will be advantageous for future work geared toward further understanding the central role of this enzyme in human disease (e.g., cardiovascular disease,[15] cancer,[22] and psychiatric disorders[21]), developing new therapeutics that target EndoV,[15, 21-22] and advancing applications of EndoV in biotechnology.[25-27, 76-78]

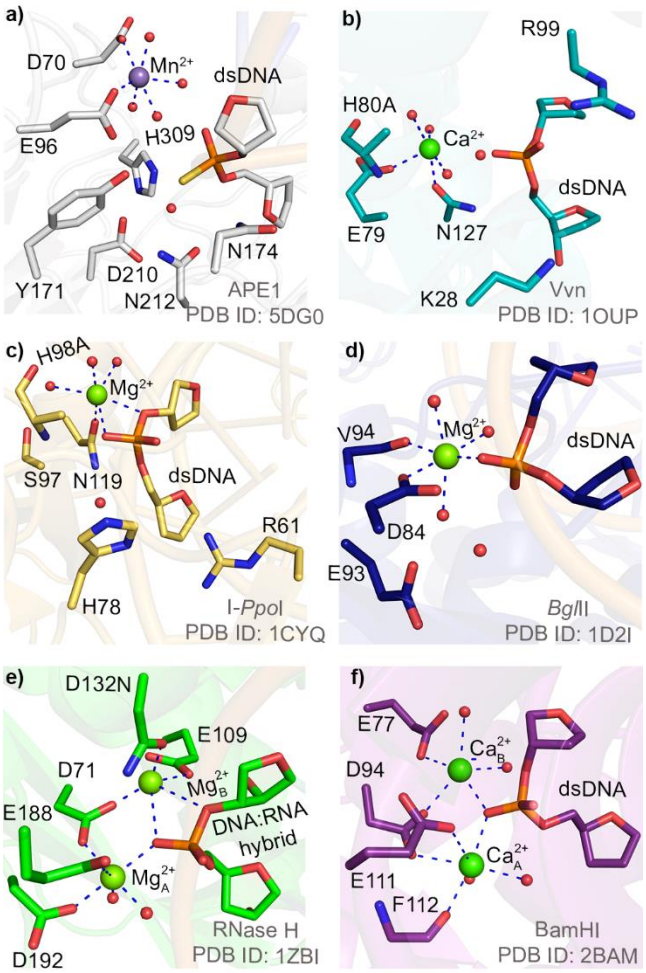

Figure 3. X-ray crystal structures of the active site in the RC for: a) APE1 bound to a thio-substituted substrate, b) the H80A mutant of Vvn, c) the H98A mutant of I-*Ppo*I, d) wild-type *Bgl*II, e) the D132N mutant of RNase H, and f) wild-type BamHI.

Computational Methodology

Model Building

Although the only available crystal structure of human EndoV is of the apoenzyme in the absence of metal cofactor/s (PDB ID: 6OZE),[28] the crystal structure of mouse EndoV exists as a homodimer that contains a double-stranded RNA (dsRNA) substrate and metal ions (two metal ions per active site, PDB ID: 6OZO).[28] Since the protein sequences of mouse (monomer) and human EndoV, including the active sites, are highly similar (81% sequence identity, Figure 1a), a model of the human EndoV–substrate complex was obtained by superimposing the crystal structures with respect to protein heavy atoms (root-mean-square deviation (RMSD) = 1.029 Å, Figure S1a) and deleting mouse EndoV, while retaining the substrate, two Mn^{2+} ions, and five directly coordinated water molecules. The five unpaired terminal nucleotides from the 5′-side of the inosine-containing RNA strand and 11 nucleotides on the 3′-side of the complementary strand were removed due to their distal location from the active site and their lack of interactions with the enzyme. Mn^{2+} ions were replaced with Mg^{2+} and four mutations in human EndoV (C140A, C225S, C226A, and C228S) were reverted using PyMOL 2.5.[79] PROPKA was used to assign protonation states to titratable amino acids at pH 7.0.[80] Three models with different metal-binding configurations found in either one or two metal-dependent nucleases (Figure 3)[28, 32, 69, 74-75] were then generated: 1) Mg_A^{2+} was removed and the remaining Mg^{2+} adopted an octahedral coordination geometry involving D52, D126, and four water molecules, while the metal formed water-mediated contacts with O3′ and a non-bridging oxygen of the scissile phosphate (denoted indirect Mg^{2+}–substrate coordination, Figure S2a); 2) Mg_A^{2+} was removed and the remaining Mg^{2+} was directly coordinated to both O3′ and a non-bridging oxygen of the scissile phosphate, as well as D52, D126, and two water molecules (denoted direct Mg^{2+}–substrate coordination, Figure S2b); and 3) two metals were retained, which are bridged by D52 and a non-bridging oxygen of the scissile phosphate (Figure S2c), while Mg_A^{2+} was also coordinated to D240 and three water molecules, and Mg_B^{2+} was also coordinated to D126, two water molecules, and O3′ of the scissile phosphate.

MD Simulations

Throughout the MD simulations, the protein and RNA were described using the AMBER ff14SB[81] and ffbsc0χOL3 force fields,[82-83] respectively. Parameters for inosine were supplemented by the generalized AMBER force field (GAFF)[84] using ANTECHAMBER 17.3,[85] while the Mg^{2+} parameters developed by Allnér *et al*.[86] were adopted. Atomic partial charges for inosine were

determined using the restrained electrostatic potential (RESP) from the R.E.D.v.III.4 program.[87] The tLEaP module of AMBER18[88] was used to neutralize the system with Na^+ ions (22 ions for one metal model and 20 ions for two metal model), and add 16 Na^+ and Cl^- ions to reach a physiological salt concentration (150 mM, which lead to a total of 16 Cl^- ions and 38 (one metal model) or 36 (two metal model) Na^+ ions), as determined using the SLTCAP calculator.[89] The entire enzyme–RNA complex was solvated in a TIP3P truncated octahedral water box, while maintaining a minimum distance of 10.0 Å between the solute and box faces.

Each system was minimized using 2500 steps of the steepest descent and 2500 steps of the conjugate gradient method in each minimization round and applying a 100 kcal mol^{-1} $Å^{-2}$ force constant to the restrained portions. The first minimization step relaxed the solvent, while restraining the solute. The second step minimized the solute hydrogen atoms, while restraining the rest of the system. The next minimization step was divided into 9 rounds to enhance substrate binding while maintaining octahedral metal coordination by gradually reducing the solute restraints based on the distance from the active site metal/s (starting with 20 Å sphere and ending at 4 Å in 2 Å increments). Subsequently, the full solute was minimized while restraining the solvent. In the final minimization step, the entire model was minimized with no restraints.

After minimization, the system was heated from 10 to 310 K in 50 K increments using a Langevin thermostat while applying a restraint of 25 kcal mol^{-1} $Å^{-2}$. Next, a 200 ps equilibration run was performed in which the restraint was relaxed from 25 to 1.5 kcal mol^{-1} $Å^{-2}$. Long-range electrostatic interactions were treated with the particle mesh Ewald method and a cut-off of 10 Å from the edge of the solute was used for non-bonding interactions. The SHAKE algorithm was used to restrain all bonds containing a hydrogen atom. While applying the periodic boundary condition, triplicate 500 ns MD production simulations were performed using a NPT ensemble (Berendsen barostat). The hydrogen-bond distances between the heavy atoms in the four base pairs on the terminal end of the 3′-side of inosine were restrained using a force constant of 25 kcal mol^{-1} $Å^{-2}$ to prevent dsRNA unravelling during production simulations.

The CPPTRAJ module (V18.01) of the AMBER 2018 suite was used to analyze the MD trajectories.[88] For all hydrogen bond analysis, a hydrogen bond was considered to be present when the distance between the heavy atoms was < 3.4 Å and the hydrogen-bond angle was > 120°. Backbone RMSD was determined with respect to the first simulation frame. The active site RMSD

was calculated using the heavy atoms of D52, D126, D240, E100, K155, the nucleotides containing the scissile phosphate moiety (A250 and U251), and the 3′-flanking nucleotide of inosine (A252). The RMSDs reveal that all models are stable (Figure S3 and Table S1).

MD snapshots of catalytically-active conformations were extracted using strict distance-based criteria (Figure S4 and Table S2). In particular, a Mg^{2+}-ligated water was considered to be in position for leaving group protonation when the distance between the water oxygen and O3′ of A250 was < 3.5 Å. Mg^{2+} was considered to be appropriately positioned to facilitate leaving group departure when ≤ 2.5 Å from O3′. A water molecule was considered to be available for nucleophilic attack when the oxygen was < 4.0 Å from the phosphorus reaction centre. D240 was considered to be available to activate the water nucleophile when Oδ of D240 is < 7.5 Å from the phosphorus reaction centre. A water chain was determined to bridge D240 (Oδ) and the phosphorous reaction centre when oxygen of the second water was simultaneously within 3.5 Å of D240 and the oxygen of the nucleophilic water.

QM/MM Calculations

QM/MM was used to map the catalytic pathway starting from each MD snapshot chosen as discussed in the previous section. The ONIOM formalism[90] was used due to previous successes of this methodology in characterizing the chemical pathways for many enzymes,[57, 63, 91-94] including metalloenzymes[91, 95-101] and nucleases.[45, 47-48, 57, 63, 102-103] For mechanisms involving a single metal, the QM region included Mg^{2+} and the directly coordinated D52, D126, and three water molecules, as well as an additional water molecule either directly coordinated to Mg^{2+} or hydrogen bonded to E100 (Figure S5a–b). The QM region also includes D240, E100, K155, the nucleotides containing the scissile phosphate moiety (A250 and U251), and an adjacent phosphate on the 3′ side of inosine (A252), leading to a total of 122 QM atoms and a QM region charge of –3. The MM region is composed of the remaining EndoV–RNA complex and any surrounding water molecules with an atom within 6 Å of the enzyme or substrate, which resulted in 2357 (direct Mg^{2+}–substrate coordination) or 2368 (indirect Mg^{2+}–substrate coordination) water molecules and an overall charge of –22. For mechanisms involving two metals, the QM region contained Mg_A^{2+} and Mg_B^{2+}, all coordinated residues, including D52, three water molecules and D240 for Mg_A^{2+}, and 2 water molecules and D126 (in a bidentate manner) as well as the substrate and an additional

water molecule or the O3′-leaving group for Mg_B^{2+} (Figure S5c–d). An additional water hydrogen bonding to D240 was also included in the QM region, along with E100, K155, the nucleotides containing the scissile phosphate moiety (A250 and U251), and an adjacent phosphate on the 3′ side of inosine (A252), which lead to 129 QM atoms and a charge of –1. The MM region was composed as per the single metal models, which led to 2314 water molecules and an overall charge of –20. In all models, the QM/MM boundary was placed between Cα and Cβ for the amino acids, and between C4′ and C5′ for the A250 and A252 nucleotides. The hydrogen link atom approach was used to satisfy the valence of the QM atoms at the QM/MM boundary.

The B3LYP-D3(BJ)/6-31G(d,p) level of theory was used to describe the QM region of each model, while the AMBER force field (ff14Sb for EndoV[81] and ffbsc0χOL3 for RNA[82-83]) was used to describe the MM region. Because of our desire to map multiple pathways at a highly accurate level of theory with a sizable QM region, mechanical embedding was implemented, which has been previously successfully used to describe phosphodiester bond hydrolysis catalyzed by other metalloenzymes,[104-108] including nucleases.[57, 62-63, 109-110] Indeed, previous computational work on nucleases,[57, 109] including bacterial EndoV,[62] revealed insignificant differences between the geometries and energy barriers obtained using mechanical and electrostatic embedding. From each optimized reactant complex (RC), scans of key reaction parameters (i.e., distances corresponding to the strongest bonds being formed (nucleophilic attack, r(O_w···P)) and broken (P–O bond cleavage r(P–O3′))) were performed to obtain initial guesses for transition states (TSs). Each reaction parameter was increased/decreased in 0.10–0.15 Å increments. Specifically, for concerted pathways, r(O_w···P) was successively reduced, and the bond was subsequently frozen to the distance corresponding to a maximum on the potential energy surface, while r(P–O3′) was consecutively increased. For stepwise mechanisms, r(O_w···P) was first successively decreased to obtain a guess for TS1, and r(P–O3′) was then elongated in the corresponding intermediate complex (IC, obtained from TS1) to obtain a guess for TS2. Subsequently, full TS optimizations were performed for all models, followed by scans on key reaction distances (i.e., r(O_w···P) and r(P–O3′)) to obtain the corresponding RC, IC, and/or product complex (PC), which were then fully optimized. For stepwise pathways, the scans of key distances (r(O_w···P) and r(P–O3′)) from TS1 and TS2 resulted in structurally and energetically similar ICs (within 6 kJ/mol, Figure S6), verifying the pathways are connected. The nature of each minimum (all positive frequencies) and TS (single imaginary frequency) was determined using frequency calculations performed at the

same level of theory as the optimizations, which also afforded the Gibbs energy corrections. Single-point energy calculations were carried out at the ONIOM(M06-2X/6-311+G(2df,p):AMBER) level of theory to obtain the relative energies.

All QM/MM calculations were performed using Gaussian 16 (revision B.01).[111]

Results and Discussion

The barrier for the single metal-mediated human EndoV pathway involving indirect (water-mediated) Mg^{2+}–substrate coordination exceeds the typical P–O bond cleavage barrier for nucleases.

As mentioned in the introduction, an X-ray crystal structure of the PC from wild-type bacterial EndoV shows a single metal in the active site (Figure 1d).[29] Although bacterial EndoV has been proposed to use H214 as the general base to activate the water nucleophile,[62] sequence alignment indicates that an aspartate residue (D240) replaces histidine in human EndoV (Figure 1a). Other single-metal dependent nucleases have been proposed to use aspartate to activate the water nucleophile.[42, 45, 49, 57, 63-64] For example, a crystal structure of a thio-substituted RC analogue of APE1 highlights a single Mn^{2+} ion indirectly coordinated to a non-bridging oxygen of the scissile phosphate through a water molecule, and D210 appropriately positioned to aid P–O bond hydrolysis (Figure 3a).[74] QM cluster and QM/MM calculations further verified that APE1 favours water-mediated Mg^{2+} coordination to both a non-bridging oxygen and the O3′-leaving group of the scissile phosphate, and D210 activates the water nucleophile in the preferred mechanism of action.[57] Similar water-mediated coordination occurs between the metal and a non-bridging phosphate oxygen in an RC analogue of single-metal dependent Vvn (Figure 3b).[70] Therefore, a human EndoV model involving one Mg^{2+} indirectly (water-mediated) coordinated to the substrate was initially investigated.

During MD simulations, Mg^{2+} maintains an octahedral coordination geometry fulfilled by D52, D126, and four water molecules (Figure 4a and Table S3). A water molecule is consistently found on average 3.4 ± 0.1 Å from the phosphorus reaction center (Figure 4b and Table S2). Furthermore, D240 is located in proximity to the electrophilic site ($r(O\delta_{D240}\cdots P)$ = 6.8 ± 1.3 Å) and therefore available to initiate hydrolysis for 71% of the simulation time. Despite the flexibility

of the active site (Figure S3), a Mg^{2+}-ligated water molecule is suitably positioned with respect to O3′ to facilitate leaving group departure for 25% of the simulation trajectory (Figure 4b and Table S2). Finally, a second metal-ligated water is aligned to position the substrate and provide charge stabilization through hydrogen bonding to a non-bridging scissile phosphate oxygen throughout the MD simulations (91% occupancy). Thus, the human EndoV–substrate complex frequently adopts a catalytically conducive conformation.

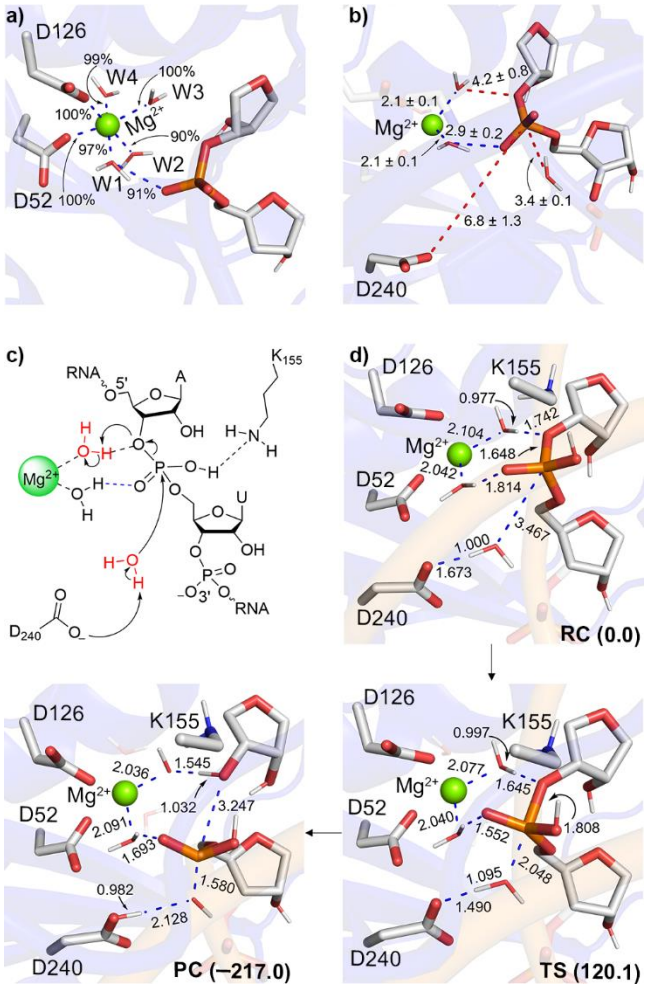

Figure 4. Key data for human EndoV-mediated phosphodiester bond cleavage involving a single metal indirectly (water-mediated) coordinated to a non-bridging phosphate oxygen of the scissile phosphate, including a) average Mg^{2+} coordination distances (Å; occupancies (%) in parentheses) and b) representative MD structure highlighting key reaction parameters (Å) across all MD replicas, as well as the c) proposed reaction pathway and d) key reaction parameters (Å) for each stationary point. Relative Gibbs energies (kJ/mol) are provided in parentheses. See Figure S7a for additional reaction parameters.

The QM/MM optimized RC from a representative MD snapshot maintains all key interactions necessary for the reaction to proceed (Figures 4c–d and S7a). Furthermore, K155 provides additional substrate charge stabilization, donating a proton to the other non-bridging oxygen of the scissile phosphate and hydrogen bonding with the newly formed H–O group throughout the reaction. From the RC, nucleophilic attack occurs concomitantly with P–O3′ bond dissociation (Figures 4c–d and S7a). The TS occurs before full proton transfer from the water nucleophile to D240 and Mg^{2+}-coordinated water to O3′, and the P–O bond is slightly (~0.15 Å) lengthened. However, despite literature precedence for an indirect (water-mediated) metal–substrate binding architecture in the active site of other nucleases (e.g., APE1[57, 63] and Vvn,[70] Figure 3a–b), the energy barrier associated with the corresponding configuration for human EndoV (120.1 kJ/mol, Figure 4d) is above typical barriers reported for metalloenzyme facilitated P–O bond cleavage (~58–96 kJ/mol).[28, 74, 112-115] This suggests that this pathway is unlikely, a conclusion in line with previous MD and QM/MM calculations on bacterial EndoV.[62] Therefore, alternate metal-coordination architectures must be considered.

Charge stabilization of the non-bridging oxygen of the scissile phosphate by direct Mg^{2+} coordination renders the human EndoV one-metal mediated P–O bond cleavage pathway catalytically feasible.

Structural data highlights that single-metal dependent nucleases can adopt many unique metal–substrate binding architectures (Figures 3 and S8).[29, 69-73, 75] The higher than anticipated barrier for P–O bond cleavage in the previous single-metal mediated mechanism for human EndoV could be lowered through enhanced substrate charge stabilization, which could be provided through direct coordination of the metal to the substrate. Indeed, X-ray crystallographic data for various one-metal dependent nucleases, including I-*Ppo*I (Figure 3c),[69] Hpy188I (Figure S8a),[73] T4 endonuclease VII (Figure S8b),[72] and I-HmuI (Figure S8c),[71] reveal direct metal coordination to both the O3′-leaving group and a non-bridging oxygen of the scissile phosphate. However, at the beginning of MD production simulations on a human EndoV RC with this metal–substrate ligation, Mg^{2+} immediately loses direct coordination to O3′, with water occupying the space between the metal and the O3′-leaving group (Figures 5a–b). Nevertheless, direct metal coordination to a non-bridging phosphate oxygen is maintained throughout the simulation (100%

occupancy). The same metal-binding architecture has been seen in crystal structures of single-metal dependent *Bgl*II (Figure 3d)[75] and *Eco*RI (Figure S8d),[116] as well as computational studies on bacterial EndoV[62] and the endonuclease domain of influenza polymerase.[61] In this active site configuration for human EndoV (Figure 5b and Table S2), Mg^{2+} remains coordinated to the substrate (2.0 ± 0.1 Å) throughout the MD simulations, while the Mg^{2+}-ligated water falls < 3.5 Å from O3′ for 40% of the simulation time. Water adopts a position for nucleophilic attack (3.5 ± 0.1 Å from electrophilic phosphorus) and D240 is suitably situated to activate the nucleophile ($r(O\delta_{D240}\cdots P)$ = 7.3 ± 0.9 Å). In complement to metal–substrate ligation, the octahedral coordination sphere of Mg^{2+} is filled by three water molecules, D52, and D126 (Figure 5a and Table S3), reflecting the experimentally-reported inactive D52A mutant.[17-18]

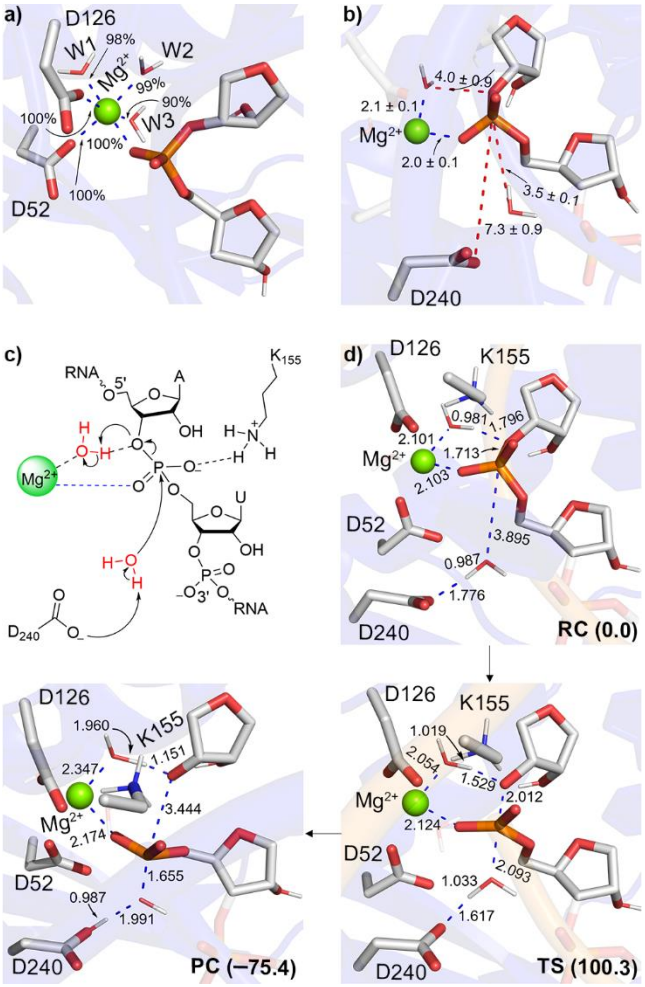

Figure 5. Key data for human EndoV-mediated phosphodiester bond cleavage involving a single metal directly coordinated to a non-bridging phosphate oxygen of the scissile phosphate, including

a) average Mg^{2+} coordination distances (Å; occupancies (%) in parentheses) and b) representative MD structure highlighting key reaction parameters (Å) across all MD replicas, as well as the c) proposed reaction pathway and d) key reaction parameters (Å) for each stationary point. Relative Gibbs energies (kJ/mol) are provided in parentheses. See Figure S7b for additional reaction parameters.

The structural features of the human EndoV RC observed in MD simulations are preserved upon QM/MM optimizations (Figure 5c–d and S7b). Furthermore, the majority of the QM/MM structural parameters along the concerted pathway for P–O bond cleavage are maintained with a change from indirect to direct metal–nonbridging oxygen coordination. The enhanced substrate charge stabilization provided by direct Mg^{2+}–substrate coordination ensures K155 remains cationic throughout the reaction pathway, while providing additional substrate charge stabilization through hydrogen bonding. As a result, the catalytic barrier decreases by 19.8 kJ/mol upon conversion from indirect to direct metal–substrate coordination, leading to a phosphodiester bond cleavage barrier ($\Delta^{\ddagger}G$ = 100.3 kJ/mol) close to the experimentally-observed barriers for a range of nucleases (~58–96 kJ/mol),[28, 74, 112-115] including mouse EndoV (84.5 kJ/mol).[28] The energetic feasibility of the human EndoV pathway involving direct metal–substrate coordination correlates with a more stable active site across the MD simulation trajectories for this metal binding geometry (Figure S3d and Table S1) and increased residency of a catalytically-active conformation (Table S2). The proposal that the catalytic step of human EndoV can proceed in the presence of one metal adds to growing literature suggesting that a single metal may be enough to cleave the phosphodiester backbone of nucleic acids.[51-57, 62-64, 67-68]

Regardless of the mode of leaving group stabilization, the two-metal mediated P–O bond cleavage pathway for human EndoV is catalytically viable.

Although bacterial EndoV has been shown to utilize a single metal for phosphodiester bond cleavage[29, 62, 113] and our calculations suggest that human EndoV can similarly follow a one-metal dependent pathway, the activity of mouse EndoV depends on two catalytic Mg^{2+} ions.[28] Since the active sites of mouse and human EndoV contain the same catalytic residues (Figure 1a), and the general two-metal mediated mechanism is widely accepted for nucleic acid backbone cleavage,[28, 30-50] the ability of human EndoV to use two metals to break the P–O bond of dsRNA was

considered. Throughout MD simulations, the human EndoV active site was significantly more stable in the presence of two metals compared to a single metal (Figure S3). The two metals remain ~ 4 Å apart (Figure 6a and Table S3), which correlates with the ~ 3.9 Å separation proposed for two-metal mediated RNA hydrolysis mechanisms.[117] Furthermore, a water molecule is properly positioned with respect to the phosphorus reaction center for nucleophilic attack for 99% of the simulations ($r(O_W \cdots P) = 3.2 \pm 0.1$ Å), while maintaining coordination to Mg_A^{2+} ($r(O_W \cdots Mg_A^{2+}) = 2.1 \pm 0.1$ Å, Figure 6b). A second water molecule bridges the nucleophile and D240 for 54% of the simulation time (Table S2), which could facilitate nucleophilic attack ($r(O_W \cdots O_{\text{bridging water}}) = 3.0 \pm 0.3$ Å and $r(O\delta_{D240} \cdots O_{\text{bridging water}}) = 2.9 \pm 0.3$ Å). This suggests that two metals are well accommodated in the active site of human EndoV when bound to the dsRNA substrate, while maintaining a catalytically conducive conformation.

In terms of metal coordination, the Mg^{2+} ions are bridged by D52 throughout the simulations, correlating with the observation that mutation of this residue to alanine kills enzyme activity.[17-18] The remaining Mg_A^{2+} octahedral coordination is fulfilled by three water molecules, D240, and a non-bridging oxygen of the scissile phosphate. Although two water molecules and D126 (bidentate coordination) are also bound to Mg_B^{2+}, two Mg_B^{2+}–substrate coordination configurations occur (Figure 6a and Tables S2–S3). First, unlike the single-metal human EndoV model, 75 ns of the MD simulation trajectory maintained direct Mg_B^{2+}–O3′ ligation for the two-metals model. This metal–substrate binding configuration mirrors that observed in X-ray crystal structures of other two-metal mediated nucleases, including RNase H (Figure 3e),[30] AaRNase III (Figure S8e),[31] HindIII (Figure S8f),[41] and retroviral integrase (Figure S8g).[37] Second, a water molecule intervenes between Mg_B^{2+} and the O3′-leaving group for the remainder of the simulation time ($r(O3' \cdots O_W) = 3.3 \pm 0.4$ Å, Figure 6b). This metal-binding architecture has been observed in X-ray crystallographic data for two-metal dependent BamHI (Figure 3f),[32] MutH (Figure S8h),[40] and BgII (Figure S8i).[39] Due to the persistence of two metal-binding configurations in the human EndoV active site, which each correspond to architectures previously reported in the nuclease literature, MD snapshots corresponding to both metal–substrate coordination geometries were used to initiate QM/MM calculations.

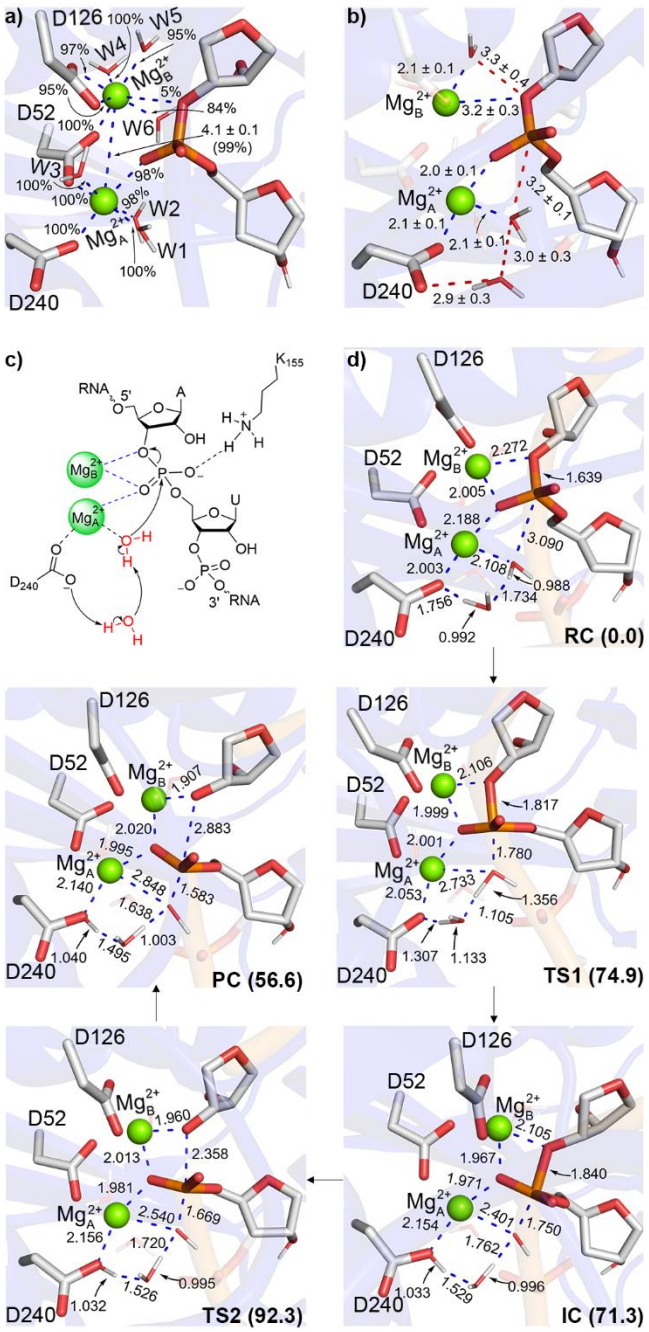

Figure 6. a) Average Mg^{2+} coordination distances (Å; occupancies (%) in parentheses) and b) representative MD structure highlighting key reaction parameters (Å) across all MD replicas, as well as the c) proposed reaction pathway and d) key reaction parameters (Å) for each stationary point along the human EndoV-mediated phosphodiester bond cleavage involving two metals with direct Mg_B^{2+}–O3′ coordination. Relative Gibbs energies (kJ/mol) are provided in parentheses. See Figure S9 for additional reaction parameters.

When an MD snapshot corresponding to direct Mg_B^{2+}–O3′ coordination was considered, the metal binding architecture is generally preserved upon QM/MM optimization, with the exception of Mg_B^{2+} adopting penta-coordination due to monodentate (rather than bidentate) binding of D126 (Figures 6c–d and S9). A similar Mg_B^{2+} penta-coordination geometry was observed in the crystal structure of RNase H (Figure 3e).[30] The phosphodiester bond cleavage follows a stepwise mechanism (Figure 6c–d and S9). In the first step, water nucleophilic attack on the phosphorus reaction center is coupled with proton transfer from the nucleophile to metal-coordinated D240 through a bridging water. While Mg_A^{2+} becomes penta-coordinated in TS1 due to the loss of water nucleophile coordination, Mg_B^{2+} reverts to an octahedral binding configuration due to bidentate coordination of D126. K155 donates a proton to a non-bridging oxygen of the scissile phosphate moiety in TS1 to help stabilize increased charge on the substrate. This change in metal binding architecture and protonation of the substrate parallels that reported in a previous QM/MM MD study of two-metal dependent *Bacillus halodurans* RNase H.[44] These structural features result in a barrier of 74.9 kJ/mol and a slightly (3.6 kJ/mol) stabilized phosphorane intermediate. In the second reaction step, the phosphodiester bond significantly elongates (r(P–O3′) increases by 0.5 Å compared to IC) and the proton on the non-bridging oxygen of the scissile phosphate to return to K155. The associated rate-determining barrier is 92.3 kJ/mol. When an MD snapshot with indirect (water-mediated) metal coordination to the substrate was considered, both metals maintain octahedral coordination geometry throughout the stepwise reaction pathway (Figure 7 and S10). More importantly, most reaction parameters are preserved across both two-metal mediated mechanisms characterized in the present work, leading to similar rate-determining barriers regardless of the Mg_B^{2+}–O3′ coordination mode (within 3.3 kJ/mol, Figures 6 and 7). Thus, irrespective of whether direct or indirect (water-mediated) Mg_B^{2+} coordination to the O3′ leaving group occurs, our predicted barriers for the two-metal mediated human EndoV pathway fall within the range of the experimental barriers reported for other nucleases (~58–96 kJ/mol),[28, 74, 112-115] including mouse EndoV (84.5 kJ/mol),[28] and the computed human EndoV–substrate structures are also consistent with X-ray crystallographic data for mouse EndoV (Figure S11). Overall, our calculations predict that human EndoV can make use of two metal-binding positions in the active site to facilitate P–O bond cleavage. We note that phosphodiester bond cleavage is followed by product release, which commonly involves metal ion migration coupled with active site rearrangement for both one- and two-metal dependent nucleases.[46, 51-52, 55, 67, 118-119] For some two-

metal mediated nucleases,[120-124] including mouse EndoV,[28] a third metal has been suggested to move into the active site during product formation to facilitate product release. Since the present work is solely focused on the P–O bond cleavage step, the role of the third metal was not explicitly investigated.

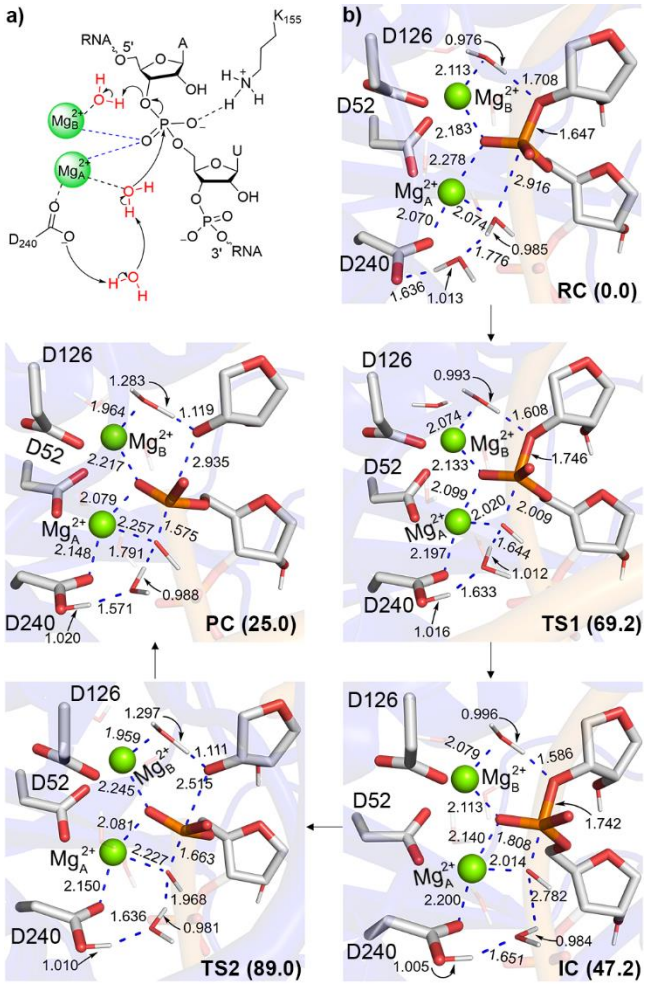

Figure 7. a) The proposed reaction pathway and b) key reaction parameters (Å) for each stationary point along the human EndoV-mediated phosphodiester bond cleavage involving two metals with indirect (water-mediated) Mg_B^{2+}–O3′ coordination. Relative Gibbs energies (kJ/mol) are provided in parentheses. See Figure S10 for additional reaction parameters.

Human EndoV can uniquely use either one or two metals to catalyze cleavage of the highly stable phosphodiester bond.

The present study is an important step toward understanding the catalytic mechanism of human EndoV due to limited existing data. In fact, the only currently available X-ray crystal structure of human EndoV does not contain the substrate or metal cofactor/s (Figure 1b)[28] and no kinetic studies have been conducted. As a result, our MD simulations provide the first picture of the human EndoV–substrate complex in the presence of active site metal cofactor/s and show the stability of the complex for a range of metal binding architectures. Our QM/MM calculations highlight that human EndoV can use a single metal to mediate phosphodiester bond cleavage. Indeed, although a mechanism involving indirect (water-mediated) metal coordination to the leaving group and nonbridging oxygen of the substrate results in a barrier well above those observed for other nucleases (Figure 4),[28, 74, 112-115] improved substrate charge stabilization afforded by direct metal coordination to the nonbridging oxygen of the scissile phosphate coupled with indirect coordination to the O3′-leaving group renders the one-metal mediated pathway energetically feasible (Figure 5). In our proposed single-metal dependent human EndoV mechanism, an active site aspartate residue (D240) acts as the general base to activate the water nucleophile, the metal aids leaving group departure by activating a water molecule that protonates O3′, and an active site lysine (K155) along with the metal facilitate substrate positioning and charge stabilization. Our computed geometries correlate with structural data for other members of the EndoV family (Figure S11a) and our data clarify the observed loss in catalytic activity upon D52A mutation,[17-18] with D52 being a key metal binding residue.

Our proposal that human EndoV can facilitate the phosphodiester bond cleavage in the presence of a single metal parallels suggestions made for bacterial EndoV,[29, 62, 125] as well as many other nucleases including APE1,[57, 63-64] I-*Ppo*I,[69, 115, 126] Hpy188I,[73] T4 endonuclease VII,[72] I-HmuI,[71] Vvn,[70] *Eco*RI,[116] and *Bgl*ll (Figures 3 and S8).[75] In all cases, one metal is proposed to be enough for the nuclease to facilitate the extremely challenging P–O bond cleavage due to the presence of a strong general base in the active site, namely a histidine (bacterial EndoV, I-*Ppo*I, T4 endonuclease VII, Vvn, I-HmuI), aspartate (APE1, human EndoV), tyrosine (Hpy188I), or a neighboring phosphate moiety of the substrate (*Eco*RI). Nevertheless, the metal–substrate coordination geometry and therefore intricate details of the mechanism can vary between these

enzymes due to differences in active site compositions. For example, the weaker general base in bacterial (histidine) compared to human (aspartate) EndoV results in an active site lysine playing a more active role in bacteria (i.e., general acid rather than substrate charge stabilization, Figure 8). Alternatively, despite many nucleases containing an active site aspartate residue that likely initiates the reaction (e.g., APE1 (D210),[57, 63-64] RNase P (D399),[42] *Eco*RV (D90),[45] and HIV-1 reverse transcriptase (D185[49])), different active site compositions alter the fine details of the chemical pathway. For example, the availability of a weaker acid to stabilize the charge on the scissile phosphate (lysine versus protonated histidine) renders the indirect metal coordination to the second nonbridging oxygen observed in APE1 unable to promote human EndoV activity, which necessitates direct metal coordination (Figure 8). Perhaps more importantly, although active site composition diversity can result in subtle mechanistic deviations, our calculations contribute to the growing body of literature, including computational support,[57, 62-64] that suggests catalytic cleavage of phosphodiester bonds is feasible in the presence of a single active site metal.[51, 54-55, 67-68]

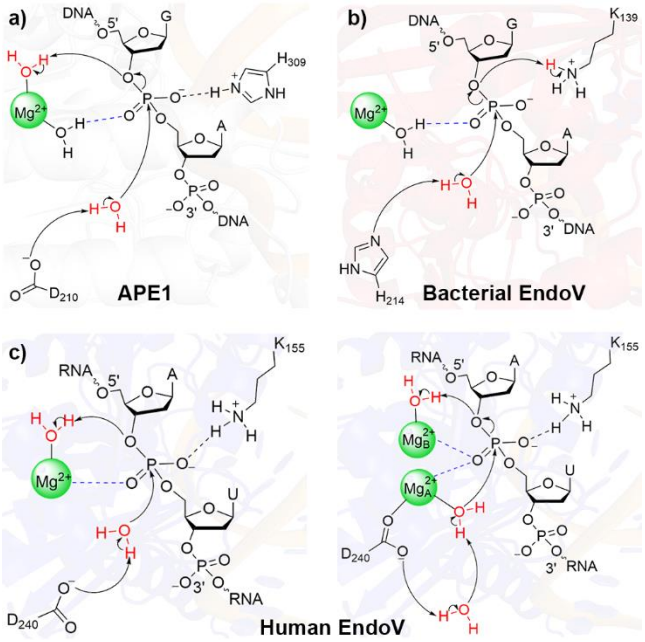

Figure 8. The proposed phosphodiester bond cleavage pathway for a) APE1,[57, 63-64] b) bacterial EndoV,[62] and c) one (left) and two-metal mediated (right) human EndoV as characterized in the present work.

To complement one metal mediated catalysis, our calculations suggest that human EndoV can efficiently facilitate phosphodiester bond cleavage in the presence of two metals, regardless of the metal–substrate (leaving group) coordination geometry (Figures 6 and 7). In these mechanisms, the first metal (Mg_A^{2+}) triggers activation of the nucleophilic water, D240 facilitates proton abstraction from the Mg_A^{2+}-coordinated water nucleophile with help of a bridging water molecule, and the second metal (Mg_B^{2+}) aids leaving group departure through either direct coordination or activation of a water molecule for O3′ protonation. The two metals along with K155 stabilize the charge on the substrate. Both mechanisms are consistent with crystallographic data for mouse EndoV (Figure S11b–c), which has a similar active site composition (Figure 1a). Furthermore, both metal binding architectures have been reported for other nucleases, with direct metal–leaving group coordination observed for RNase H (Figure 3e),[30] AaRNase III (Figure S9e),[31] HindIII (Figure S8f),[41] and retroviral integrase (Figure S8g),[37] and water-mediated Mg_B^{2+}–O3′ coordination observed for BamHI (Figure 3f),[32] MutH (Figure S8h),[40] and BgII (Figure S8i).[39] Although direct metal coordination to the leaving group is less persistent in the active site according to MD simulations on the RC, the unique behavior that different metal binding architectures are possible may arise due to the additional charge stabilization afforded by K155 in the human EndoV active site compared to the charge stabilization being restricted to the metals for other two-metal mediated nucleases.[30-32, 37, 40]

While the crystal structure of bacterial EndoV displays a single metal (Figure 1d)[29] and mouse EndoV shows two metals (Figure 1c)[28] in the active site, our calculations reveal that human EndoV can invoke either one or two metals for catalysis. Although the barrier for single-metal mediated catalysis is slightly larger than that for the two-metal dependent pathways, the final number of metals utilized likely depends on the metal ion concentration among other considerations. This proposal is supported by experimentally-reported metal concentration dependent behaviour of PvuII endonuclease.[67] Specifically, although the X-ray crystal structure of PvuII endonuclease contains two metals in the active site (Figure S8j),[34] P–O bond cleavage rates as a function of metal ion concentration fit both one-metal and two-metal ion models.[67] Therefore, the enzyme was suggested to use only one metal ion at low metal concentrations, but a more efficient two-metal mediated catalysis under saturating metal ion conditions. Similarly, while one metal is essential for human EndoV catalytic activity, the enzyme can benefit from the use of two metals due to the presence of two suitable Mg^{2+} binding positions in the active site. To the best of

our knowledge, our work is the first computational study to provide direct mechanistic comparisons between one- and two-metal mediated P–O bond cleavage reactions in the same active site architecture. Our work highlights that while some enzymes may use either one[29, 69-73, 75] or two[28, 30-41] metals for phosphodiester bond hydrolysis in nucleic acids (Figures 3 and S8), some enzymes have the ability to exploit both pathways, thus bringing a fresh perspective to the one versus two metal ion controversy. Our calculations thereby emphasize that it is important to bear in mind that there might not be an unequivocal answer for some nucleases regarding the number of metals required to catalyze phosphodiester bond cleavage, with the composition of the enzyme active site and metal concentration playing significant roles in determining the metal ion stoichiometry requirements for catalysis.

Conclusion

The present work has used MD simulations and QM/MM calculations to afford the first proposed mechanism of action for human EndoV. MD simulations were initially used to reveal the structure of the human EndoV–substrate complex in the presence of metal cofactor/s, which highlighted the stability of the complex in the presence of a range of active site metal binding architectures. Subsequently, four unique phosphodiester bond cleavage pathways were characterized using QM/MM calculations. Although a mechanism involving indirect (water-mediated) coordination of the metal to the substrate results in a barrier well above the experimentally-determined activation energy for a range of other nucleases,[28, 74, 112-115] direct metal coordination to the nonbridging oxygen of the scissile phosphate coupled with indirect metal coordination to the O3′ leaving group yields an energetically feasible pathway for single-metal mediated catalysis. In our predicted mechanism, D240 activates the nucleophilic water, a Mg^{2+}-ligated water protonates the leaving group, and substrate charge stabilization is provided by both the directly coordinated Mg^{2+} and K155. Nevertheless, our calculations predict that human EndoV can also accommodate two metals in the active site and use both metals to facilitate the P–O bond cleavage. In the two-metal mediated mechanism, the first metal (Mg_A^{2+}) activates the nucleophilic water while D240 abstracts the proton from the Mg_A^{2+}-coordinated water nucleophile with help of a bridging water molecule, and the second metal (Mg_B^{2+}) promotes leaving group departure either through direct coordination or activation of a water molecule to protonate O3′. The two metals

along with K155 stabilize the charge on the substrate throughout the reaction. Thus, in line with experimental literature for another nuclease (PvuII endonuclease),[67] while one metal is essential for human EndoV catalytic activity, the enzyme can benefit from the use of two metals, with the final number of metals utilized likely depending on the local metal ion concentration among other considerations. To the best of our knowledge, this is the first computational study that has provided direct evidence that a given endonuclease can utilize both one and two-metal dependent mechanisms to cleave phosphodiester bonds in nucleic acids, thus emphasizing that researchers must bear in mind that there may not be an unequivocal answer regarding metal ion stoichiometry requirements for catalysis and adding a unique perspective to the existing one versus two metal controversy in the literature. The mechanistic details of human EndoV function uncovered in the present work are vital for further discerning the central role of this enzyme in human disease (e.g., cardiovascular disease,[15] cancer,[22] and psychiatric disorders),[21] developing new therapeutics that target EndoV,[15, 21-22] and refining uses of EndoV in biotechnology.[25-27, 76-78]

ASSOCIATED CONTENT

Corresponding Author

Stacey D. Wetmore*

ORCID iD: http://orcid.org/0000-0002-5801-3942

Affiliation: Department of Chemistry and Biochemistry, University of Lethbridge, 4401 University Drive West, Lethbridge, Alberta, Canada T1K 3M4

stacey.wetmore@uleth.ca

Author Information

Rajwinder Kaur

ORCID iD: http://orcid.org/0000-0001-9349-4924

Affiliation: Department of Chemistry and Biochemistry, University of Lethbridge, 4401 University Drive West, Lethbridge, Alberta, Canada T1K 3M4

rajwinder.kaur@uleth.ca

Notes

The authors declare no competing financial interest.

Supporting Information:

Additional information for comparisons of mouse and apo-human EndoV structures and the human EndoV QM/MM model (Figure S1), starting models for MD simulations (Figure S2), RMSDs (Figure S3 and Table S1), MD snapshots used to build QM/MM models (Figure S4), QM regions of all QM/MM models (Figure S5), comparisons of QM/MM ICs for two-metal mediated mechanisms (Figure S6), chemical mechanisms and key structural parameters for QM/MM stationary points (Figures S7, S9, and S10), representative crystal structures of one- and two-metal dependent nucleases (Figure S8), comparisons of human EndoV QM/MM RCs and mouse EndoV crystal structure (Figure S11), and percent occupancies of reaction parameters and average metal coordination distances from MD simulations (Tables S2 and S3).

Acknowledgements

S.D.W. thanks the Natural Sciences and Engineering Research Council of Canada (NSERC; 2016-04568) and the Canada Research Chairs program (2021-00484) for financial support. R.K thanks Alberta Innovates – Technology Futures, and the University of Lethbridge Board of Governors and School of Graduate Studies for student scholarships. Computer resources were provided by Digital Research Alliance of Canada, and Advanced Research Computing (ARC) at the University of Calgary.

References

(1) Kuraoka, I., Diversity of endonuclease V: From DNA repair to RNA editing. *Biomolecules* **2015,** *5* (4), 2194–2206.

(2) Schouten, K. A.; Weiss, B., Endonuclease V protects *Escherichia coli* against specific mutations caused by nitrous acid. *Mutat. Res.* **1999,** *435* (3), 245–254.

(3) Gott, J. M.; Emeson, R. B., Functions and mechanisms of RNA editing. *Annu. Rev. Genet.* **2000,** *34* (1), 499–531.

(4) Pang, B.; McFaline, J. L.; Burgis, N. E.; Dong, M.; Taghizadeh, K.; Sullivan, M. R.; Elmquist, C. E.; Cunningham, R. P.; Dedon, P. C., Defects in purine nucleotide metabolism lead to substantial incorporation of xanthine and hypoxanthine into DNA and RNA. *Proc. Natl. Acad. Sci. U.S.A.* **2012,** *109* (7), 2319–2324.

(5) Behmanesh, M.; Sakumi, K.; Abolhassani, N.; Toyokuni, S.; Oka, S.; Ohnishi, Y.; Tsuchimoto, D.; Nakabeppu, Y., ITPase-deficient mice show growth retardation and die before weaning. *Cell Death Differ.* **2009,** *16* (10), 1315–1322.

(6) Bass, B. L., RNA editing by adenosine deaminases that act on RNA. *Annu. Rev. Biochem.* **2002,** *71* (1), 817–846.

(7) Nishikura, K., Functions and regulation of RNA editing by ADAR deaminases. *Annu. Rev. Biochem.* **2010,** *79*, 321–349.

(8) Farajollahi, S.; Maas, S., Molecular diversity through RNA editing: a balancing act. *Trends Genet.* **2010,** *26* (5), 221–230.

(9) Han, L.; Diao, L.; Yu, S.; Xu, X.; Li, J.; Zhang, R.; Yang, Y.; Werner, H. M.; Eterovic, A. K.; Yuan, Y., The genomic landscape and clinical relevance of A-to-I RNA editing in human cancers. *Cancer cell* **2015,** *28* (4), 515–528.

(10) Paz, N.; Levanon, E. Y.; Amariglio, N.; Heimberger, A. B.; Ram, Z.; Constantini, S.; Barbash, Z. S.; Adamsky, K.; Safran, M.; Hirschberg, A., Altered adenosine-to-inosine RNA editing in human cancer. *Genome Res.* **2007,** *17* (11), 1586–1595.

(11) Srivastava, P. K.; Bagnati, M.; Delahaye-Duriez, A.; Ko, J.-H.; Rotival, M.; Langley, S. R.; Shkura, K.; Mazzuferi, M.; Danis, B.; van Eyll, J., Genome-wide analysis of differential RNA editing in epilepsy. *Genome Res.* **2017,** *27* (3), 440–450.

(12) Hosaka, T.; Tsuji, H.; Kwak, S., RNA editing: A new therapeutic target in amyotrophic lateral sclerosis and other neurological diseases. *Int. J. Mol. Sci.* **2021,** *22* (20), 10958.

(13) Tran, S. S.; Jun, H.-I.; Bahn, J. H.; Azghadi, A.; Ramaswami, G.; Van Nostrand, E. L.; Nguyen, T. B.; Hsiao, Y.-H. E.; Lee, C.; Pratt, G. A., Widespread RNA editing dysregulation in brains from autistic individuals. *Nat. Neurosci.* **2019,** *22* (1), 25–36.

(14) Khermesh, K.; D'Erchia, A. M.; Barak, M.; Annese, A.; Wachtel, C.; Levanon, E. Y.; Picardi, E.; Eisenberg, E., Reduced levels of protein recoding by A-to-I RNA editing in Alzheimer's disease. *RNA* **2016,** *22* (2), 290–302.

(15) Kong, X. Y.; Huse, C.; Yang, K.; Øgaard, J.; Berges, N.; Vik, E. S.; Nawaz, M. S.; Quiles-Jiménez, A.; Abbas, A.; Gregersen, I., Endonuclease V regulates atherosclerosis through C-C motif chemokine ligand 2-mediated monocyte infiltration. *J. Am. Heart Assoc.* **2021,** *10* (14), e020656.

(16) Breen, M. S.; Dobbyn, A.; Li, Q.; Roussos, P.; Hoffman, G. E.; Stahl, E.; Chess, A.; Sklar, P.; Li, J. B.; Devlin, B., Global landscape and genetic regulation of RNA editing in cortical samples from individuals with schizophrenia. *Nat. Neurosci.* **2019,** *22* (9), 1402–1412.

(17) Morita, Y.; Shibutani, T.; Nakanishi, N.; Nishikura, K.; Iwai, S.; Kuraoka, I., Human endonuclease V is a ribonuclease specific for inosine-containing RNA. *Nat. Commun.* **2013,** *4*, 2273.

(18) Vik, E. S.; Nawaz, M. S.; Andersen, P. S.; Fladeby, C.; Bjoras, M.; Dalhus, B.; Alseth, I., Endonuclease V cleaves at inosines in RNA. *Nat. Commun.* **2013,** *4*, 2271.

(19) Zhang, Z.; Hao, Z.; Wang, Z.; Li, Q.; Xie, W., Structure of human endonuclease V as an inosine-specific ribonuclease. *Acta Crystallogr., Sect. D: Biol. Crystallogr.* **2014,** *70* (9), 2286–2294.

(20) Cao, W., Endonuclease V: an unusual enzyme for repair of DNA deamination. *Cell. Mol. Life Sci.* **2013,** *70* (17), 3145–3156.

(21) Rajkumar, A. P.; Christensen, J. H.; Mattheisen, M.; Jacobsen, I.; Bache, I.; Pallesen, J.; Grove, J.; Qvist, P.; McQuillin, A.; Gurling, H. M., Analysis of t (9; 17)(q33. 2; q25. 3) chromosomal breakpoint regions and genetic association reveals novel candidate genes for bipolar disorder. *Bipolar Disord.* **2015,** *17* (2), 205–211.

(22) Kong, X. Y.; Vik, E. S.; Nawaz, M. S.; Berges, N.; Dahl, T. B.; Vågbø, C.; Suganthan, R.; Segers, F.; Holm, S.; Quiles-Jiménez, A., Deletion of Endonuclease V suppresses chemically induced hepatocellular carcinoma. *Nucleic Acids Res.* **2020,** *48* (8), 4463–4479.

(23) Knutson, S. D.; Arthur, R. A.; Johnston, H. R.; Heemstra, J. M., Selective enrichment of A-to-I edited transcripts from cellular RNA using Endonuclease V. *J. Am. Chem. Soc.* **2020,** *142* (11), 5241–5251.

(24) Knutson, S. D.; Arthur, R. A.; Johnston, H. R.; Heemstra, J. M., Direct immunodetection of global A-to-I RNA editing activity with a chemiluminescent bioassay. *Angew. Chem. Int. Ed.* **2021,** *60* (31), 17009–17017.

(25) Chang, Y.; Huang, Z.; Quan, H.; Li, H.; Yang, S.; Song, Y.; Wang, J.; Yuan, J.; Wu, C., Construction of a DNA damage repair gene signature for predicting prognosis and immune response in breast cancer. *Front. Oncol.* **2022,** *12*, 1085632.

(26) Huang, J.; Kirk, B.; Favis, R.; Soussi, T.; Paty, P.; Cao, W.; Barany, F., An endonuclease/ligase based mutation scanning method especially suited for analysis of neoplastic tissue. *Oncogene* **2002,** *21* (12), 1909–1921.

(27) Pincas, H.; Pingle, M. R.; Huang, J.; Lao, K.; Paty, P. B.; Friedman, A. M.; Barany, F., High sensitivity EndoV mutation scanning through real-time ligase proofreading. *Nucleic Acids Res.* **2004,** *32* (19), e148.

(28) Wu, J.; Samara, N. L.; Kuraoka, I.; Yang, W., Evolution of inosine-specific endonuclease V from bacterial DNase to eukaryotic RNase. *Mol. Cell* **2019,** *76* (1), 44–56.

(29) Dalhus, B.; Arvai, A. S.; Rosnes, I.; Olsen, Ø. E.; Backe, P. H.; Alseth, I.; Gao, H.; Cao, W.; Tainer, J. A.; Bjørås, M., Structures of endonuclease V with DNA reveal initiation of deaminated adenine repair. *Nat. Struct. Mol. Biol.* **2009,** *16*, 138–143.

(30) Nowotny, M.; Gaidamakov, S. A.; Crouch, R. J.; Yang, W., Crystal structures of RNase H bound to an RNA/DNA hybrid: substrate specificity and metal-dependent catalysis. *Cell* **2005,** *121* (7), 1005–1016.

(31) Gan, J.; Shaw, G.; Tropea, J. E.; Waugh, D. S.; Court, D. L.; Ji, X., A stepwise model for double-stranded RNA processing by ribonuclease III. *Mol. Microbiol.* **2007,** *67* (1), 143–154.

(32) Viadiu, H.; Aggarwal, A. K., The role of metals in catalysis by the restriction endonuclease Bam HI. *Nat. Struct. Biol.* **1998,** *5* (10), 910–916.

(33) Deibert, M.; Grazulis, S.; Sasnauskas, G.; Siksnys, V.; Huber, R., Structure of the tetrameric restriction endonuclease NgoMIV in complex with cleaved DNA. *Nat. Struct. Biol.* **2000,** *7* (9), 792–799.

(34) Horton, J. R.; Cheng, X., PvuII endonuclease contains two calcium ions in active sites. *J. Mol. Biol.* **2000,** *300* (5), 1049–1056.

(35) Dunten, P. W.; Little, E. J.; Gregory, M. T.; Manohar, V. M.; Dalton, M.; Hough, D.; Bitinaite, J.; Horton, N. C., The structure of SgrAI bound to DNA; recognition of an 8 base pair target. *Nucleic Acids Res.* **2008,** *36* (16), 5405–5416.

(36) Lambert, A. R.; Sussman, D.; Shen, B.; Maunus, R.; Nix, J.; Samuelson, J.; Xu, S.-Y.; Stoddard, B. L., Structures of the rare-cutting restriction endonuclease NotI reveal a unique metal binding fold involved in DNA binding. *Structure* **2008,** *16* (4), 558–569.

(37) Hare, S.; Maertens, G. N.; Cherepanov, P., 3′-Processing and strand transfer catalysed by retroviral integrase in crystallo. *EMBO J.* **2012,** *31* (13), 3020–3028.

(38) Hiller, D. A.; Rodriguez, A. M.; Perona, J. J., Non-cognate enzyme–DNA complex: structural and kinetic analysis of EcoRV endonuclease bound to the EcoRI recognition site GAATTC. *J. Mol. Biol.* **2005,** *354* (1), 121–136.

(39) Newman, M.; Lunnen, K.; Wilson, G.; Greci, J.; Schildkraut, I.; Phillips, S. E., Crystal structure of restriction endonuclease BglI bound to its interrupted DNA recognition sequence. *EMBO J.* **1998,** *17* (18), 5466–5476.

(40) Lee, J. Y.; Chang, J.; Joseph, N.; Ghirlando, R.; Rao, D. N.; Yang, W., MutH complexed with hemi- and unmethylated DNAs: coupling base recognition and DNA cleavage. *Mol. Cell* **2005,** *20* (1), 155–166.

(41) Watanabe, N.; Takasaki, Y.; Sato, C.; Ando, S.; Tanaka, I., Structures of restriction endonuclease HindIII in complex with its cognate DNA and divalent cations. *Acta Crystallogr. D Biol. Crystallogr.* **2009,** *65* (12), 1326–1333.

(42) Howard, M. J.; Klemm, B. P.; Fierke, C. A., Mechanistic studies reveal similar catalytic strategies for phosphodiester bond hydrolysis by protein-only and RNA-dependent ribonuclease P. *J. Biol. Chem.* **2015,** *290* (21), 13454–13464.

(43) Mordasini, T.; Curioni, A.; Andreoni, W., Why do divalent metal ions either promote or inhibit enzymatic reactions? The case of BamHI restriction endonuclease from combined quantum-classical simulations. *J. Biol. Chem.* **2003,** *278* (7), 4381–4384.

(44) De Vivo, M.; Dal Peraro, M.; Klein, M. L., Phosphodiester cleavage in ribonuclease H occurs via an associative two-metal-aided catalytic mechanism. *J. Am. Chem. Soc.* **2008,** *130* (33), 10955–10962.

(45) Imhof, P.; Fischer, S.; Smith, J. C., Catalytic mechanism of DNA backbone cleavage by the restriction enzyme *Eco*RV: A quantum mechanical/molecular mechanical analysis. *Biochemistry* **2009,** *48* (38), 9061–9075.

(46) Rosta, E.; Nowotny, M.; Yang, W.; Hummer, G., Catalytic mechanism of RNA backbone cleavage by ribonuclease H from quantum mechanics/molecular mechanics simulations. *J. Am. Chem. Soc.* **2011,** *133* (23), 8934–8941.

(47) Ribeiro, A. J. M.; Ramos, M. J.; Fernandes, P. A., The catalytic mechanism of HIV-1 Integrase for DNA 3′-end processing established by QM/MM calculations. *J. Am. Chem. Soc.* **2012,** *134* (32), 13436–13447.

(48) Araujo, A. R.; Ribeiro, A. J.; Fernandes, P. A.; Ramos, M. J., Catalytic mechanism of retroviral integrase for the strand transfer reaction explored by QM/MM calculations. *J. Chem. Theory Comput.* **2014,** *10* (12), 5458–5466.

(49) Rungrotmongkol, T.; Mulholland, A. J.; Hannongbua, S., QM/MM simulations indicate that Asp185 is the likely catalytic base in the enzymatic reaction of HIV-1 reverse transcriptase. *MedChemComm* **2014,** *5* (5), 593–596.

(50) Casalino, L.; Nierzwicki, L.; Jinek, M.; Palermo, G., Catalytic mechanism of non-target DNA cleavage in CRISPR-Cas9 revealed by *Ab initio* molecular dynamics. *ACS Catal.* **2020,** *10* (22), 13596–13605.

(51) Yang, W.; Lee, J. Y.; Nowotny, M., Making and breaking nucleic acids: two-Mg^{2+}-ion catalysis and substrate specificity. *Mol. Cell* **2006,** *22* (1), 5–13.

(52) Dupureur, C. M., Roles of metal ions in nucleases. *Curr. Opin. Chem. Biol.* **2008,** *12* (2), 250–255.

(53) Dupureur, C. M., An integrated look at metallonuclease mechanism. *Curr. Chem. Biol.* **2008,** *2* (2), 159–173.

(54) Yang, W., An equivalent metal ion in one- and two-metal-ion catalysis. *Nat. Struct. Mol. Biol.* **2008,** *15* (11), 1228–1231.

(55) Dupureur, C. M., One is enough: Insights into the two-metal ion nuclease mechanism from global analysis and computational studies. *Metallomics* **2010,** *2* (9), 609–620.

(56) Cowan, J. A., Metal-mediated hydrolysis of biological phosphate esters: a critical analysis of the essential metal ion stoichiometry for magnesium-dependent nuclease activation. *J. Biol. Inorg. Chem.* **1997,** *2* (2), 168–176.

(57) Aboelnga, M. M.; Wetmore, S. D., Unveiling a single-metal-mediated phosphodiester bond cleavage mechanism for nucleic acids: A multiscale computational investigation of a human DNA repair enzyme. *J. Am. Chem. Soc.* **2019,** *141* (21), 8646–8656.

(58) Pitts, S. L.; Liou, G. F.; Mitchenall, L. A.; Burgin, A. B.; Maxwell, A.; Neuman, K. C.; Osheroff, N., Use of divalent metal ions in the DNA cleavage reaction of topoisomerase IV. *Nucleic Acids Res.* **2011,** *39* (11), 4808-4817.

(59) Donati, E.; Genna, V.; De Vivo, M., Recruiting mechanism and functional role of a third metal ion in the enzymatic activity of 5′ structure-specific nucleases. *J. Am. Chem. Soc.* **2020,** *142* (6), 2823–2834.

(60) Onishi, I.; Sunaba, S.; Yoshida, N.; Hirata, F.; Irisa, M., Role of Mg^{2+} ions in DNA hydrolysis by *EcoRV* studied by the 3D-reference interaction site model and molecular dynamics. *J. Phys. Chem. B* **2018,** *122* (39), 9061-9075.

(61) Xiao, S.; Klein, M. L.; LeBard, D. N.; Levine, B. G.; Liang, H.; MacDermaid, C. M.; Alfonso-Prieto, M., Magnesium-dependent RNA binding to the PA endonuclease domain of the avian influenza polymerase. *J. Phys. Chem. B* **2014,** *118* (4), 873–889.

(62) Kaur, R.; Wetmore, S. D., Is metal stabilization of the leaving group required or can lysine facilitate phosphodiester bond cleavage in nucleic acids? A computational study of EndoV. *J. Chem. Inf. Model.* **2024,** *64* (3), 944-959.

(63) Kaur, R.; Aboelnga, M. M.; Nikkel, D. J.; Wetmore, S. D., The metal dependence of single-metal mediated phosphodiester bond cleavage: A QM/MM study of a multifaceted human enzyme. *Phys. Chem. Chem. Phys.* **2022,** *24* (47), 29130–29140.

(64) Kaur, R.; Nikkel, D. J.; Aboelnga, M. M.; Wetmore, S. D., The impact of DFT functional, cluster model size, and implicit solvation on the structural description of single-metal-mediated DNA phosphodiester bond cleavage: The case study of APE1. *The Journal of Physical Chemistry B* **2022,** *126* (50), 10672–10683.

(65) Onishi, I.; Sunaba, S.; Yoshida, N.; Hirata, F.; Irisa, M., Role of Mg2+ Ions in DNA Hydrolysis by EcoRV, Studied by the 3D-Reference Interaction Site Model and Molecular Dynamics. *J. Phys. Chem. B.* **2018,** *122* (39), 9061-9075.

(66) Raper, A. T.; Reed, A. J.; Suo, Z., Kinetic mechanism of DNA polymerases: Contributions of conformational dynamics and a third divalent metal ion. *Chem. Rev.* **2018,** *118* (12), 6000–6025.

(67) Xie, F.; Qureshi, S. H.; Papadakos, G. A.; Dupureur, C. M., One- and two-metal ion catalysis: Global single-turnover kinetic analysis of the PvuII endonuclease mechanism. *Biochemistry* **2008,** *47* (47), 12540–12550.

(68) Pingoud, V.; Wende, W.; Friedhoff, P.; Reuter, M.; Alves, J.; Jeltsch, A.; Mones, L.; Fuxreiter, M.; Pingoud, A., On the divalent metal ion dependence of DNA cleavage by restriction endonucleases of the *Eco*RI family. *J. Mol. Biol.* **2009,** *393* (1), 140–160.

(69) Galburt, E. A.; Chevalier, B.; Tang, W.; Jurica, M. S.; Flick, K. E.; Monnat, R. J.; Stoddard, B. L., A novel endonuclease mechanism directly visualized for I-*Ppo*I. *Nat. Struct. Biol.* **1999,** *6* (12), 1096–1099.

(70) Li, C. L.; Hor, L. I.; Chang, Z. F.; Tsai, L. C.; Yang, W. Z.; Yuan, H. S., DNA binding and cleavage by the periplasmic nuclease Vvn: A novel structure with a known active site. *EMBO J.* **2003,** *22* (15), 4014–4025.

(71) Shen, B. W.; Landthaler, M.; Shub, D. A.; Stoddard, B. L., DNA binding and cleavage by the HNH homing endonuclease I-HmuI. *J. Mol. Biol.* **2004,** *342* (1), 43–56.

(72) Biertümpfel, C.; Yang, W.; Suck, D., Crystal structure of T4 endonuclease VII resolving a Holliday junction. *Nature* **2007,** *449* (7162), 616–620.

(73) Sokolowska, M.; Czapinska, H.; Bochtler, M., Hpy188I–DNA pre- and post-cleavage complexes snapshots of the GIY-YIG nuclease mediated catalysis. *Nucleic Acids Res.* **2011,** *39* (4), 1554–1564.

(74) Freudenthal, B. D.; Beard, W. A.; Cuneo, M. J.; Dyrkheeva, N. S.; Wilson, S. H., Capturing snapshots of APE1 processing DNA damage. *Nat. Struct. Mol. Biol.* **2015,** *22* (11), 924–931.

(75) Lukacs, C. M.; Kucera, R.; Schildkraut, I.; Aggarwal, A. K., Understanding the immutability of restriction enzymes: crystal structure of BglII and its DNA substrate at 1.5 Å resolution. *Nat. Struct. Mol. Biol.* **2000,** *7* (2), 134–140.

(76) Miyazaki, K., Random DNA fragmentation with endonuclease V: application to DNA shuffling. *Nucleic Acids Res.* **2002,** *30* (24), e139.

(77) Turner, D. J.; Pingle, M. R.; Barany, F., Harnessing asymmetrical substrate recognition by thermostable EndoV to achieve balanced linear amplification in multiplexed SNP typing. *Biochem. Cell Biol.* **2006,** *84* (2), 232–242.

(78) Wang, Z.; Wang, H.-Y.; Feng, H., A simple and reproducible method for directed evolution: combination of random mutation with dITP and DNA fragmentation with endonuclease V. *Mol. Biotechnol.* **2013,** *53*, 49–54.

(79) DeLano, W. L., Pymol: An open-source molecular graphics tool. *CCP4 Newsl. Protein Crystallogr* **2002,** *40* (1), 82–92.

(80) Rostkowski, M.; Olsson, M. H. M.; Søndergaard, C. R.; Jensen, J. H., Graphical analysis of pH-dependent properties of proteins predicted using PROPKA. *BMC Struct. Biol.* **2011,** *11* (1), 1–6.

(81) Maier, J. A.; Martinez, C.; Kasavajhala, K.; Wickstrom, L.; Hauser, K. E.; Simmerling, C., ff14SB: Improving the accuracy of protein side chain and backbone parameters from ff99SB. *J. Chem. Theory Comput.* **2015,** *11* (8), 3696–3713.

(82) Zgarbová, M.; Otyepka, M.; Šponer, J. i.; Mládek, A. t.; Banáš, P.; Cheatham III, T. E.; Jurecka, P., Refinement of the Cornell et al. nucleic acids force field based on reference quantum chemical calculations of glycosidic torsion profiles. *J. Chem. Theory Comput.* **2011,** *7* (9), 2886–2902.

(83) Pérez, A.; Marchán, I.; Svozil, D.; Sponer, J.; Cheatham, T. E.; Laughton, C. A.; Orozco, M., Refinement of the AMBER force field for nucleic acids: Improving the description of α/γ conformers. *Biophys. J.* **2007,** *92* (11), 3817–3829.

(84) Wang, J.; Wolf, R. M.; Caldwell, J. W.; Kollman, P. A.; Case, D. A., Junmei Wang, Romain M. Wolf, James W. Caldwell, Peter A. Kollman, and David A. Case," Development and testing of a general amber force field" *J. Comput. Chem.* **2004,** *25* (9), 1157–1174.

(85) Wang, J.; Wang, W.; Kollman, P. A.; Case, D. A., Automatic atom type and bond type perception in molecular mechanical calculations. *J. Mol. Graph. Model.* **2006,** *25* (2), 247–260.

(86) Allnér, O.; Nilsson, L.; Villa, A., Magnesium ion–water coordination and exchange in biomolecular simulations. *J. Chem. Theory Comput.* **2012,** *8* (4), 1493–1502.

(87) Dupradeau, F.-Y.; Pigache, A.; Zaffran, T.; Savineau, C.; Lelong, R.; Grivel, N.; Lelong, D.; Rosanski, W.; Cieplak, P., The REd. Tools: Advances in RESP and ESP charge derivation and force field library building. *Phys. Chem. Chem. Phys.* **2010,** *12* (28), 7821–7839.

(88) Case, D.; Ben-Shalom, I.; Brozell, S.; Cerutti, D.; Cheatham III, T.; Cruzeiro, V.; Darden, T.; Duke, R.; Ghoreishi, D.; Gilson, M., AMBER 2018; 2018. *University of California, San Francisco* **2018**.

(89) Schmit, J. D.; Kariyawasam, N. L.; Needham, V.; Smith, P. E., SLTCAP: A simple method for calculating the number of ions needed for MD simulation. *J. Chem. Theory Comput.* **2018,** *14* (4), 1823–1827.

(90) Chung, L. W.; Sameera, W. M. C.; Ramozzi, R.; Page, A. J.; Hatanaka, M.; Petrova, G. P.; Harris, T. V.; Li, X.; Ke, Z.; Liu, F.; Li, H.-B.; Ding, L.; Morokuma, K., The ONIOM method and its applications. *Chem. Rev.* **2015,** *115* (12), 5678-5796.

(91) Geronimo, I.; Vidossich, P.; Donati, E.; De Vivo, M., Computational investigations of polymerase enzymes: Structure, function, inhibition, and biotechnology. *Wiley Interdiscip. Rev. Comput. Mol. Sci.* **2021,** *11* (6), e1534.

(92) Castro-Amorim, J.; Oliveira, A.; Mukherjee, A. K.; Ramos, M. J.; Fernandes, P. A., Unraveling the reaction mechanism of russell's viper venom factor X activator: a paradigm for the reactivity of zinc metalloproteinases? *J. Chem. Inf. Model.* **2023,** *63*, 4056–4069.

(93) Gérard, E. F.; Mokkawes, T.; Johannissen, L. O.; Warwicker, J.; Spiess, R. R.; Blanford, C. F.; Hay, S.; Heyes, D. J.; de Visser, S. P., How is substrate halogenation triggered by the vanadium haloperoxidase from *Curvularia inaequalis*? *ACS Catal.* **2023,** *13*, 8247–8261.

(94) Shirazi, J.; Jafari, S.; Ryde, U.; Irani, M., Catalytic reaction mechanism of glyoxalase II: A quantum mechanics/molecular mechanics study. *J. Phys. Chem. B* **2023,** *127*, 4480–4495.

(95) Perera, L.; Freudenthal, B. D.; Beard, W. A.; Pedersen, L. G.; Wilson, S. H., Revealing the role of the product metal in DNA polymerase β catalysis. *Nucleic Acids Res.* **2017,** *45* (5), 2736–2745.

(96) Medina, F. E.; Jaña, G. A., QM/MM study of a VIM-1 metallo-β-lactamase enzyme: The catalytic reaction mechanism. *ACS Catal.* **2021,** *12* (1), 36–47.

(97) Balhara, R.; Chatterjee, R.; Jindal, G., A computational approach to understand the role of metals and axial ligands in artificial heme enzyme catalyzed C–H insertion. *Phys. Chem. Chem. Phys.* **2021,** *23* (15), 9500–9511.

(98) Chaturvedi, S. S.; Ramanan, R.; Hu, J.; Hausinger, R. P.; Christov, C. Z., Atomic and electronic structure determinants distinguish between ethylene formation and l-arginine hydroxylation reaction mechanisms in the ethylene-forming enzyme. *ACS Catal.* **2021,** *11* (3), 1578–1592.

(99) Paul, A.; Mishra, S., Metal-ion promiscuity of microbial enzyme DapE at its second metal-binding site. *J. Biol. Inorg. Chem.* **2021,** *26*, 569-582.

(100) Garcia-Borràs, M.; Kan, S. J.; Lewis, R. D.; Tang, A.; Jimenez-Osés, G.; Arnold, F. H.; Houk, K. N., Origin and control of chemoselectivity in cytochrome c catalyzed carbene transfer into Si–H and N–H bonds. *J. Am. Chem. Soc.* **2021,** *143* (18), 7114–7123.

(101) Bras, N. F.; Fernandes, P. A.; Ramos, M. J., QM/MM studies on the β-galactosidase catalytic mechanism: hydrolysis and transglycosylation reactions. *J. Chem. Theory Comput.* **2010,** *6* (2), 421–433.

(102) Yanagita, H.; Urano, E.; Matsumoto, K.; Ichikawa, R.; Takaesu, Y.; Ogata, M.; Murakami, T.; Wu, H.; Chiba, J.; Komano, J., Structural and biochemical study on the inhibitory activity of derivatives of 5-nitro-furan-2-carboxylic acid for RNase H function of HIV-1 reverse transcriptase. *Bioorg. Med. Chem.* **2011,** *19* (2), 816–825.

(103) Elsässer, B.; Fels, G., Atomistic details of the associative phosphodiester cleavage in human ribonuclease H. *Phys. Chem. Chem. Phys.* **2010,** *12* (36), 11081–11088.

(104) Paul, A.; Mishra, S., Metal–ion promiscuity of microbial enzyme DapE at its second metal-binding site. *J. Biol. Inorg. Chem.* **2021,** *26*, 569-582.

(105) Bras, N. F.; Fernandes, P. A.; Ramos, M. J., QM/MM studies on the β-galactosidase catalytic mechanism: Hydrolysis and transglycosylation reactions. *J. Chem. Theory Comput.* **2010,** *6* (2), 421-433.

(106) Jayasinghe-Arachchige, V. M.; Hu, Q.; Sharma, G.; Paul, T. J.; Lundberg, M.; Quinonero, D.; Parac-Vogt, T. N.; Prabhakar, R., Hydrolysis of chemically distinct sites of human serum albumin by polyoxometalate: A hybrid QM/MM (ONIOM) study. *J. Comput. Chem.* **2019,** *40* (1), 51-61.

(107) Tolbert, A. E.; Ervin, C. S.; Ruckthong, L.; Paul, T. J.; Jayasinghe-Arachchige, V. M.; Neupane, K. P.; Stuckey, J. A.; Prabhakar, R.; Pecoraro, V. L., Heteromeric three-stranded coiled coils designed using a Pb (II)$(Cys)_3$ template mediated strategy. *Nat. Chem.* **2020,** *12* (4), 405-411.

(108) Garcia-Borràs, M.; Kan, S. J.; Lewis, R. D.; Tang, A.; Jimenez-Osés, G.; Arnold, F. H.; Houk, K. N., Origin and control of chemoselectivity in cytochrome c catalyzed carbene transfer into Si–H and N–H bonds. *J. Am. Chem. Soc.* **2021,** *143* (18), 7114-7123.

(109) Kaur, R.; Frederickson, A.; Wetmore, S. D., Elucidation of the catalytic mechanism of a single-metal dependent homing endonuclease using QM and QM/MM approaches: The case study of I-*Ppo*I. *Phys. Chem. Chem. Phys.* **2024,** *26*, 8919-8931.

(110) Juliano, S. A.; Serafim, L. F.; Duay, S. S.; Heredia Chavez, M.; Sharma, G.; Rooney, M.; Comert, F.; Pierce, S.; Radulescu, A.; Cotten, M. L., A potent host defense peptide triggers DNA damage and is active against multidrug-resistant gram-negative pathogens. *ACS Infect. Dis.* **2020,** *6* (5), 1250-1263.

(111) Frisch, M.; Trucks, G.; Schlegel, H.; Scuseria, G.; Robb, M.; Cheeseman, J.; Scalmani, G.; Barone, V.; Petersson, G.; Nakatsuji, H., Gaussian 16 Rev. B. 01, Wallingford, CT. **2016**.

(112) Wu, H.; Lima, W. F.; Crooke, S. T., Investigating the structure of human RNase H1 by site-directed mutagenesis. *J. Biol. Chem.* **2001,** *276* (26), 23547–23553.

(113) Feng, H.; Klutz, A. M.; Cao, W., Active site plasticity of endonuclease V from Salmonella typhimurium. *Biochemistry* **2005,** *44* (2), 675–683.

(114) Gong, S.; Yu, H. H.; Johnson, K. A.; Taylor, D. W., DNA unwinding is the primary determinant of CRISPR-Cas9 activity. *Cell Rep.* **2018,** *22* (2), 359–371.

(115) Eastberg, J. H.; Eklund, J.; Monnat, R.; Stoddard, B. L., Mutability of an HNH nuclease imidazole general base and exchange of a deprotonation mechanism. *Biochemistry* **2007,** *46* (24), 7215–7225.

(116) Jeltsch, A.; Alves, J.; Wolfes, H.; Maass, G.; Pingoud, A., Substrate-assisted catalysis in the cleavage of DNA by the *Eco*RI and *Eco*RV restriction enzymes. *Proc. Natl. Acad. Sci. U.S.A.* **1993,** *90* (18), 8499–8503.

(117) Steitz, T. A.; Steitz, J. A., A general two-metal-ion mechanism for catalytic RNA. *Proc. Natl. Acad. Sci. U. S. A.* **1993,** *90* (14), 6498–502.

(118) Oezguen, N.; Schein, C. H.; Peddi, S. R.; Power, T. D.; Izumi, T.; Braun, W., A "moving metal mechanism" for substrate cleavage by the DNA repair endonuclease APE-1. *Proteins* **2007,** *68* (1), 313-323.

(119) He, H.; Chen, Q.; Georgiadis, M. M., High-resolution crystal structures reveal plasticity in the metal binding site of apurinic/apyrimidinic endonuclease I. *Biochemistry* **2014,** *53* (41), 6520-6529.

(120) Donati, E.; Genna, V.; De Vivo, M., Recruiting mechanism and functional role of a third metal ion in the enzymatic activity of 5′ structure-specific nucleases. *J. Am. Chem. Soc.* **2020,** *142* (6), 2823-2834.

(121) Dùrr, S. L.; Bohuszewicz, O.; Berta, D.; Suardiaz, R.; Jambrina, P. G.; Peter, C.; Shao, Y.; Rosta, E., The role of conserved residues in the DEDDh motif: The proton-transfer mechanism of HIV-1 RNase H. *ACS Catal.* **2021,** *11* (13), 7915-7927.

(122) Nakamura, T.; Zhao, Y.; Yamagata, Y.; Hua, Y.-j.; Yang, W., Watching DNA polymerase η make a phosphodiester bond. *Nature* **2012,** *487* (7406), 196-201.

(123) Perera, L.; Freudenthal, B. D.; Beard, W. A.; Pedersen, L. G.; Wilson, S. H., Revealing the role of the product metal in DNA polymerase β catalysis. *Nucleic Acids Res.* **2017,** *45* (5), 2736-2745.

(124) Gao, Y.; Yang, W., Capture of a third Mg^{2+} is essential for catalyzing DNA synthesis. *Science* **2016,** *352* (6291), 1334-1337.

(125) Feng, H.; Dong, L.; Cao, W., Catalytic mechanism of endonuclease V: A catalytic and regulatory two-metal model. *Biochemistry* **2006,** *45* (34), 10251–10259.

(126) Flick, K. E.; Jurica, M. S.; Monnat, R. J.; Stoddard, B. L., DNA binding and cleavage by the nuclear intron-encoded homing endonuclease I-*Ppo*I. *Nature* **1998,** *394* (6688), 96–101.

For Table of Contents Only